

Branching fraction and charge asymmetry measurements in $B \rightarrow J/\psi \pi \pi$ decays

B. Aubert,¹ M. Bona,¹ D. Boutigny,¹ Y. Karyotakis,¹ J. P. Lees,¹ V. Poireau,¹ X. Prudent,¹ V. Tisserand,¹
A. Zghiche,¹ J. Garra Tico,² E. Grauges,² L. Lopez,³ A. Palano,³ G. Eigen,⁴ I. Ofte,⁴ B. Stugu,⁴ L. Sun,⁴
G. S. Abrams,⁵ M. Battaglia,⁵ D. N. Brown,⁵ J. Button-Shafer,⁵ R. N. Cahn,⁵ Y. Groyzman,⁵ R. G. Jacobsen,⁵
J. A. Kadyk,⁵ L. T. Kerth,⁵ Yu. G. Kolomensky,⁵ G. Kukartsev,⁵ D. Lopes Pegna,⁵ G. Lynch,⁵ L. M. Mir,⁵
T. J. Orimoto,⁵ M. Pripstein,⁵ N. A. Roe,⁵ M. T. Ronan,^{5,*} K. Tackmann,⁵ W. A. Wenzel,⁵ P. del Amo Sanchez,⁶
C. M. Hawkes,⁶ A. T. Watson,⁶ T. Held,⁷ H. Koch,⁷ B. Lewandowski,⁷ M. Pelizaeus,⁷ T. Schroeder,⁷
M. Steinke,⁷ W. N. Cottingham,⁸ D. Walker,⁸ D. J. Asgeirsson,⁹ T. Cuhadar-Donszelmann,⁹ B. G. Fulsom,⁹
C. Hearty,⁹ N. S. Knecht,⁹ T. S. Mattison,⁹ J. A. McKenna,⁹ A. Khan,¹⁰ M. Saleem,¹⁰ L. Teodorescu,¹⁰
V. E. Blinov,¹¹ A. D. Bukin,¹¹ V. P. Druzhinin,¹¹ V. B. Golubev,¹¹ A. P. Onuchin,¹¹ S. I. Serednyakov,¹¹
Yu. I. Skovpen,¹¹ E. P. Solodov,¹¹ K. Yu Todyshev,¹¹ M. Bondioli,¹² S. Curry,¹² I. Eschrich,¹² D. Kirkby,¹²
A. J. Lankford,¹² P. Lund,¹² M. Mandelkern,¹² E. C. Martin,¹² D. P. Stoker,¹² S. Abachi,¹³ C. Buchanan,¹³
S. D. Foulkes,¹⁴ J. W. Gary,¹⁴ F. Liu,¹⁴ O. Long,¹⁴ B. C. Shen,¹⁴ L. Zhang,¹⁴ H. P. Paar,¹⁵ S. Rahatlou,¹⁵
V. Sharma,¹⁵ J. W. Berryhill,¹⁶ C. Campagnari,¹⁶ A. Cunha,¹⁶ B. Dahmes,¹⁶ T. M. Hong,¹⁶ D. Kovalskyi,¹⁶
J. D. Richman,¹⁶ T. W. Beck,¹⁷ A. M. Eisner,¹⁷ C. J. Flacco,¹⁷ C. A. Heusch,¹⁷ J. Kroseberg,¹⁷ W. S. Lockman,¹⁷
T. Schalk,¹⁷ B. A. Schumm,¹⁷ A. Seiden,¹⁷ D. C. Williams,¹⁷ M. G. Wilson,¹⁷ L. O. Winstrom,¹⁷ E. Chen,¹⁸
C. H. Cheng,¹⁸ A. Dvoretzki,¹⁸ F. Fang,¹⁸ D. G. Hitlin,¹⁸ I. Narsky,¹⁸ T. Piatenko,¹⁸ F. C. Porter,¹⁸
G. Mancinelli,¹⁹ B. T. Meadows,¹⁹ K. Mishra,¹⁹ M. D. Sokoloff,¹⁹ F. Blanc,²⁰ P. C. Bloom,²⁰ S. Chen,²⁰
W. T. Ford,²⁰ J. F. Hirschauer,²⁰ A. Kreisel,²⁰ M. Nagel,²⁰ U. Nauenberg,²⁰ A. Olivas,²⁰ J. G. Smith,²⁰
K. A. Ulmer,²⁰ S. R. Wagner,²⁰ J. Zhang,²⁰ A. M. Gabareen,²¹ A. Soffer,²¹ W. H. Toki,²¹ R. J. Wilson,²¹
F. Winklmeier,²¹ Q. Zeng,²¹ D. D. Altenburg,²² E. Feltresi,²² A. Hauke,²² H. Jasper,²² J. Merkel,²² A. Petzold,²²
B. Spaan,²² K. Wacker,²² T. Brandt,²³ V. Klose,²³ H. M. Lacker,²³ W. F. Mader,²³ R. Nogowski,²³ J. Schubert,²³
K. R. Schubert,²³ R. Schwierz,²³ J. E. Sundermann,²³ A. Volk,²³ D. Bernard,²⁴ G. R. Bonneaud,²⁴ E. Latour,²⁴
V. Lombardo,²⁴ Ch. Thiebaux,²⁴ M. Verderi,²⁴ P. J. Clark,²⁵ W. Gradl,²⁵ F. Muheim,²⁵ S. Playfer,²⁵
A. I. Robertson,²⁵ Y. Xie,²⁵ M. Andreotti,²⁶ D. Bettoni,²⁶ C. Bozzi,²⁶ R. Calabrese,²⁶ A. Cecchi,²⁶ G. Cibinetto,²⁶
P. Franchini,²⁶ E. Luppi,²⁶ M. Negrini,²⁶ A. Petrella,²⁶ L. Piemontese,²⁶ E. Prencipe,²⁶ V. Santoro,²⁶ F. Anulli,²⁷
R. Baldini-Ferrolì,²⁷ A. Calcaterra,²⁷ R. de Sangro,²⁷ G. Finocchiaro,²⁷ S. Pacetti,²⁷ P. Patteri,²⁷ I. M. Peruzzi,^{27,†}
M. Piccolo,²⁷ M. Rama,²⁷ A. Zallo,²⁷ A. Buzzo,²⁸ R. Contri,²⁸ M. Lo Vetere,²⁸ M. M. Macri,²⁸ M. R. Monge,²⁸
S. Passaggio,²⁸ C. Patrignani,²⁸ E. Robutti,²⁸ A. Santroni,²⁸ S. Tosi,²⁸ K. S. Chaisanguanthum,²⁹ M. Morii,²⁹
J. Wu,²⁹ R. S. Dubitzky,³⁰ J. Marks,³⁰ S. Schenk,³⁰ U. Uwer,³⁰ D. J. Bard,³¹ P. D. Dauncey,³¹ R. L. Flack,³¹
J. A. Nash,³¹ M. B. Nikolich,³¹ W. Panduro Vazquez,³¹ P. K. Behera,³² X. Chai,³² M. J. Charles,³² U. Mallik,³²
N. T. Meyer,³² V. Ziegler,³² J. Cochran,³³ H. B. Crawley,³³ L. Dong,³³ V. Eyges,³³ W. T. Meyer,³³ S. Prell,³³
E. I. Rosenberg,³³ A. E. Rubin,³³ A. V. Gritsan,³⁴ Z. J. Guo,³⁴ C. K. Lae,³⁴ A. G. Denig,³⁵ M. Fritsch,³⁵
G. Schott,³⁵ N. Arnaud,³⁶ J. Béquilleux,³⁶ M. Davier,³⁶ G. Grosdidier,³⁶ A. Höcker,³⁶ V. Lepeltier,³⁶
F. Le Diberder,³⁶ A. M. Lutz,³⁶ S. Pruvot,³⁶ S. Rodier,³⁶ P. Roudeau,³⁶ M. H. Schune,³⁶ J. Serrano,³⁶ V. Sordini,³⁶
A. Stocchi,³⁶ W. F. Wang,³⁶ G. Wormser,³⁶ D. J. Lange,³⁷ D. M. Wright,³⁷ C. A. Chavez,³⁸ I. J. Forster,³⁸
J. R. Fry,³⁸ E. Gabathuler,³⁸ R. Gamet,³⁸ D. E. Hutchcroft,³⁸ D. J. Payne,³⁸ K. C. Schofield,³⁸ C. Touramanis,³⁸
A. J. Bevan,³⁹ K. A. George,³⁹ F. Di Lodovico,³⁹ W. Menges,³⁹ R. Sacco,³⁹ G. Cowan,⁴⁰ H. U. Flaecher,⁴⁰
D. A. Hopkins,⁴⁰ P. S. Jackson,⁴⁰ T. R. McMahon,⁴⁰ F. Salvatore,⁴⁰ A. C. Wren,⁴⁰ D. N. Brown,⁴¹ C. L. Davis,⁴¹
J. Allison,⁴² N. R. Barlow,⁴² R. J. Barlow,⁴² Y. M. Chia,⁴² C. L. Edgar,⁴² G. D. Lafferty,⁴² T. J. West,⁴²
J. I. Yi,⁴² J. Anderson,⁴³ C. Chen,⁴³ A. Jawahery,⁴³ D. A. Roberts,⁴³ G. Simi,⁴³ J. M. Tuggle,⁴³ G. Blaylock,⁴⁴
C. Dallapiccola,⁴⁴ S. S. Hertzbach,⁴⁴ X. Li,⁴⁴ T. B. Moore,⁴⁴ E. Salvati,⁴⁴ S. Saremi,⁴⁴ R. Cowan,⁴⁵ P. H. Fisher,⁴⁵
G. Sciolla,⁴⁵ S. J. Sekula,⁴⁵ M. Spitznagel,⁴⁵ F. Taylor,⁴⁵ R. K. Yamamoto,⁴⁵ S. E. Mclachlin,⁴⁶ P. M. Patel,⁴⁶
S. H. Robertson,⁴⁶ A. Lazzaro,⁴⁷ F. Palombo,⁴⁷ J. M. Bauer,⁴⁸ L. Cremaldi,⁴⁸ V. Eschenburg,⁴⁸ R. Godang,⁴⁸
R. Kroeger,⁴⁸ D. A. Sanders,⁴⁸ D. J. Summers,⁴⁸ H. W. Zhao,⁴⁸ S. Brunet,⁴⁹ D. Côté,⁴⁹ M. Simard,⁴⁹ P. Taras,⁴⁹
F. B. Viaud,⁴⁹ H. Nicholson,⁵⁰ G. De Nardo,⁵¹ F. Fabozzi,^{51,‡} L. Lista,⁵¹ D. Monorchio,⁵¹ C. Sciacca,⁵¹
M. A. Baak,⁵² G. Raven,⁵² H. L. Snoek,⁵² C. P. Jessop,⁵³ J. M. LoSecco,⁵³ G. Benelli,⁵⁴ L. A. Corwin,⁵⁴
K. K. Gan,⁵⁴ K. Honscheid,⁵⁴ D. Hufnagel,⁵⁴ H. Kagan,⁵⁴ R. Kass,⁵⁴ J. P. Morris,⁵⁴ A. M. Rahimi,⁵⁴
J. J. Regensburger,⁵⁴ R. Ter-Antonyan,⁵⁴ Q. K. Wong,⁵⁴ N. L. Blount,⁵⁵ J. Brau,⁵⁵ R. Frey,⁵⁵ O. Igonkina,⁵⁵

J. A. Kolb,⁵⁵ M. Lu,⁵⁵ R. Rahmat,⁵⁵ N. B. Sinev,⁵⁵ D. Strom,⁵⁵ J. Strube,⁵⁵ E. Torrence,⁵⁵ N. Gagliardi,⁵⁶ A. Gaz,⁵⁶ M. Margoni,⁵⁶ M. Morandin,⁵⁶ A. Pompili,⁵⁶ M. Posocco,⁵⁶ M. Rotondo,⁵⁶ F. Simonetto,⁵⁶ R. Stroili,⁵⁶ C. Voci,⁵⁶ E. Ben-Haim,⁵⁷ H. Briand,⁵⁷ J. Chauveau,⁵⁷ P. David,⁵⁷ L. Del Buono,⁵⁷ Ch. de la Vaissière,⁵⁷ O. Hamon,⁵⁷ B. L. Hartfiel,⁵⁷ Ph. Leruste,⁵⁷ J. Malclès,⁵⁷ J. Ocariz,⁵⁷ A. Perez,⁵⁷ L. Gladney,⁵⁸ M. Biasini,⁵⁹ R. Covarelli,⁵⁹ E. Manoni,⁵⁹ C. Angelini,⁶⁰ G. Batignani,⁶⁰ S. Bettarini,⁶⁰ G. Calderini,⁶⁰ M. Carpinelli,⁶⁰ R. Cenci,⁶⁰ A. Cervelli,⁶⁰ F. Forti,⁶⁰ M. A. Giorgi,⁶⁰ A. Lusiani,⁶⁰ G. Marchiori,⁶⁰ M. A. Mazur,⁶⁰ M. Morganti,⁶⁰ N. Neri,⁶⁰ E. Paoloni,⁶⁰ G. Rizzo,⁶⁰ J. J. Walsh,⁶⁰ M. Haire,⁶¹ J. Biesiada,⁶² P. Elmer,⁶² Y. P. Lau,⁶² C. Lu,⁶² J. Olsen,⁶² A. J. S. Smith,⁶² A. V. Telnov,⁶² E. Baracchini,⁶³ F. Bellini,⁶³ G. Cavoto,⁶³ A. D’Orazio,⁶³ D. del Re,⁶³ E. Di Marco,⁶³ R. Faccini,⁶³ F. Ferrarotto,⁶³ F. Ferroni,⁶³ M. Gaspero,⁶³ P. D. Jackson,⁶³ L. Li Gioi,⁶³ M. A. Mazzoni,⁶³ S. Morganti,⁶³ G. Piredda,⁶³ F. Polci,⁶³ F. Renga,⁶³ C. Voena,⁶³ M. Ebert,⁶⁴ H. Schröder,⁶⁴ R. Waldi,⁶⁴ T. Adye,⁶⁵ G. Castelli,⁶⁵ B. Franek,⁶⁵ E. O. Olaiya,⁶⁵ S. Ricciardi,⁶⁵ W. Roethel,⁶⁵ F. F. Wilson,⁶⁵ R. Aleksan,⁶⁶ S. Emery,⁶⁶ M. Escalier,⁶⁶ A. Gaidot,⁶⁶ S. F. Ganzhur,⁶⁶ G. Hamel de Monchenault,⁶⁶ W. Kozanecki,⁶⁶ M. Legendre,⁶⁶ G. Vasseur,⁶⁶ Ch. Yèche,⁶⁶ M. Zito,⁶⁶ X. R. Chen,⁶⁷ H. Liu,⁶⁷ W. Park,⁶⁷ M. V. Purohit,⁶⁷ J. R. Wilson,⁶⁷ M. T. Allen,⁶⁸ D. Aston,⁶⁸ R. Bartoldus,⁶⁸ P. Bechtel,⁶⁸ N. Berger,⁶⁸ R. Claus,⁶⁸ J. P. Coleman,⁶⁸ M. R. Convery,⁶⁸ J. C. Dingfelder,⁶⁸ J. Dorfan,⁶⁸ G. P. Dubois-Felsmann,⁶⁸ D. Dujmic,⁶⁸ W. Dunwoodie,⁶⁸ R. C. Field,⁶⁸ T. Glanzman,⁶⁸ S. J. Gowdy,⁶⁸ M. T. Graham,⁶⁸ P. Grenier,⁶⁸ C. Hast,⁶⁸ T. Hryn’ova,⁶⁸ W. R. Innes,⁶⁸ M. H. Kelsey,⁶⁸ H. Kim,⁶⁸ P. Kim,⁶⁸ D. W. G. S. Leith,⁶⁸ S. Li,⁶⁸ S. Luitz,⁶⁸ V. Luth,⁶⁸ H. L. Lynch,⁶⁸ D. B. MacFarlane,⁶⁸ H. Marsiske,⁶⁸ R. Messner,⁶⁸ D. R. Muller,⁶⁸ C. P. O’Grady,⁶⁸ A. Perazzo,⁶⁸ M. Perl,⁶⁸ T. Pulliam,⁶⁸ B. N. Ratcliff,⁶⁸ A. Roodman,⁶⁸ A. A. Salnikov,⁶⁸ R. H. Schindler,⁶⁸ J. Schwiening,⁶⁸ A. Snyder,⁶⁸ J. Stelzer,⁶⁸ D. Su,⁶⁸ M. K. Sullivan,⁶⁸ K. Suzuki,⁶⁸ S. K. Swain,⁶⁸ J. M. Thompson,⁶⁸ J. Va’vra,⁶⁸ N. van Bakel,⁶⁸ A. P. Wagner,⁶⁸ M. Weaver,⁶⁸ W. J. Wisniewski,⁶⁸ M. Wittgen,⁶⁸ D. H. Wright,⁶⁸ A. K. Yarritu,⁶⁸ K. Yi,⁶⁸ C. C. Young,⁶⁸ P. R. Burchat,⁶⁹ A. J. Edwards,⁶⁹ S. A. Majewski,⁶⁹ B. A. Petersen,⁶⁹ L. Wilden,⁶⁹ S. Ahmed,⁷⁰ M. S. Alam,⁷⁰ R. Bula,⁷⁰ J. A. Ernst,⁷⁰ V. Jain,⁷⁰ B. Pan,⁷⁰ M. A. Saeed,⁷⁰ F. R. Wappler,⁷⁰ S. B. Zain,⁷⁰ W. Bugg,⁷¹ M. Krishnamurthy,⁷¹ S. M. Spanier,⁷¹ R. Eckmann,⁷² J. L. Ritchie,⁷² A. M. Ruland,⁷² C. J. Schilling,⁷² R. F. Schwitters,⁷² J. M. Izen,⁷³ X. C. Lou,⁷³ S. Ye,⁷³ F. Bianchi,⁷⁴ F. Gallo,⁷⁴ D. Gamba,⁷⁴ M. Pelliccioni,⁷⁴ M. Bomben,⁷⁵ L. Bosisio,⁷⁵ C. Cartaro,⁷⁵ F. Cossutti,⁷⁵ G. Della Ricca,⁷⁵ L. Lanceri,⁷⁵ L. Vitale,⁷⁵ V. Azzolini,⁷⁶ N. Lopez-March,⁷⁶ F. Martinez-Vidal,⁷⁶ D. A. Milanese,⁷⁶ A. Oyanguren,⁷⁶ J. Albert,⁷⁷ Sw. Banerjee,⁷⁷ B. Bhuyan,⁷⁷ K. Hamano,⁷⁷ R. Kowalewski,⁷⁷ I. M. Nugent,⁷⁷ J. M. Roney,⁷⁷ R. J. Sobie,⁷⁷ J. J. Back,⁷⁸ P. F. Harrison,⁷⁸ T. E. Latham,⁷⁸ G. B. Mohanty,⁷⁸ M. Pappagallo,⁷⁸ H. R. Band,⁷⁹ X. Chen,⁷⁹ S. Dasu,⁷⁹ K. T. Flood,⁷⁹ J. J. Hollar,⁷⁹ P. E. Kutter,⁷⁹ Y. Pan,⁷⁹ M. Pierini,⁷⁹ R. Prepost,⁷⁹ S. L. Wu,⁷⁹ Z. Yu,⁷⁹ and H. Neal⁸⁰

(The BABAR Collaboration)

¹Laboratoire de Physique des Particules, IN2P3/CNRS et Université de Savoie, F-74941 Annecy-Le-Vieux, France

²Universitat de Barcelona, Facultat de Física, Departament ECM, E-08028 Barcelona, Spain

³Università di Bari, Dipartimento di Fisica and INFN, I-70126 Bari, Italy

⁴University of Bergen, Institute of Physics, N-5007 Bergen, Norway

⁵Lawrence Berkeley National Laboratory and University of California, Berkeley, California 94720, USA

⁶University of Birmingham, Birmingham, B15 2TT, United Kingdom

⁷Ruhr Universität Bochum, Institut für Experimentalphysik 1, D-44780 Bochum, Germany

⁸University of Bristol, Bristol BS8 1TL, United Kingdom

⁹University of British Columbia, Vancouver, British Columbia, Canada V6T 1Z1

¹⁰Brunel University, Uxbridge, Middlesex UB8 3PH, United Kingdom

¹¹Budker Institute of Nuclear Physics, Novosibirsk 630090, Russia

¹²University of California at Irvine, Irvine, California 92697, USA

¹³University of California at Los Angeles, Los Angeles, California 90024, USA

¹⁴University of California at Riverside, Riverside, California 92521, USA

¹⁵University of California at San Diego, La Jolla, California 92093, USA

¹⁶University of California at Santa Barbara, Santa Barbara, California 93106, USA

¹⁷University of California at Santa Cruz, Institute for Particle Physics, Santa Cruz, California 95064, USA

¹⁸California Institute of Technology, Pasadena, California 91125, USA

¹⁹University of Cincinnati, Cincinnati, Ohio 45221, USA

²⁰University of Colorado, Boulder, Colorado 80309, USA

²¹Colorado State University, Fort Collins, Colorado 80523, USA

²²Universität Dortmund, Institut für Physik, D-44221 Dortmund, Germany

²³Technische Universität Dresden, Institut für Kern- und Teilchenphysik, D-01062 Dresden, Germany

²⁴Laboratoire Leprince-Ringuet, CNRS/IN2P3, Ecole Polytechnique, F-91128 Palaiseau, France

²⁵University of Edinburgh, Edinburgh EH9 3JZ, United Kingdom

²⁶Università di Ferrara, Dipartimento di Fisica and INFN, I-44100 Ferrara, Italy

- ²⁷Laboratori Nazionali di Frascati dell'INFN, I-00044 Frascati, Italy
- ²⁸Università di Genova, Dipartimento di Fisica and INFN, I-16146 Genova, Italy
- ²⁹Harvard University, Cambridge, Massachusetts 02138, USA
- ³⁰Universität Heidelberg, Physikalisches Institut, Philosophenweg 12, D-69120 Heidelberg, Germany
- ³¹Imperial College London, London, SW7 2AZ, United Kingdom
- ³²University of Iowa, Iowa City, Iowa 52242, USA
- ³³Iowa State University, Ames, Iowa 50011-3160, USA
- ³⁴Johns Hopkins University, Baltimore, Maryland 21218, USA
- ³⁵Universität Karlsruhe, Institut für Experimentelle Kernphysik, D-76021 Karlsruhe, Germany
- ³⁶Laboratoire de l'Accélérateur Linéaire, IN2P3/CNRS et Université Paris-Sud 11, Centre Scientifique d'Orsay, B. P. 34, F-91898 ORSAY Cedex, France
- ³⁷Lawrence Livermore National Laboratory, Livermore, California 94550, USA
- ³⁸University of Liverpool, Liverpool L69 7ZE, United Kingdom
- ³⁹Queen Mary, University of London, E1 4NS, United Kingdom
- ⁴⁰University of London, Royal Holloway and Bedford New College, Egham, Surrey TW20 0EX, United Kingdom
- ⁴¹University of Louisville, Louisville, Kentucky 40292, USA
- ⁴²University of Manchester, Manchester M13 9PL, United Kingdom
- ⁴³University of Maryland, College Park, Maryland 20742, USA
- ⁴⁴University of Massachusetts, Amherst, Massachusetts 01003, USA
- ⁴⁵Massachusetts Institute of Technology, Laboratory for Nuclear Science, Cambridge, Massachusetts 02139, USA
- ⁴⁶McGill University, Montréal, Québec, Canada H3A 2T8
- ⁴⁷Università di Milano, Dipartimento di Fisica and INFN, I-20133 Milano, Italy
- ⁴⁸University of Mississippi, University, Mississippi 38677, USA
- ⁴⁹Université de Montréal, Physique des Particules, Montréal, Québec, Canada H3C 3J7
- ⁵⁰Mount Holyoke College, South Hadley, Massachusetts 01075, USA
- ⁵¹Università di Napoli Federico II, Dipartimento di Scienze Fisiche and INFN, I-80126, Napoli, Italy
- ⁵²NIKHEF, National Institute for Nuclear Physics and High Energy Physics, NL-1009 DB Amsterdam, The Netherlands
- ⁵³University of Notre Dame, Notre Dame, Indiana 46556, USA
- ⁵⁴Ohio State University, Columbus, Ohio 43210, USA
- ⁵⁵University of Oregon, Eugene, Oregon 97403, USA
- ⁵⁶Università di Padova, Dipartimento di Fisica and INFN, I-35131 Padova, Italy
- ⁵⁷Laboratoire de Physique Nucléaire et de Hautes Energies, IN2P3/CNRS, Université Pierre et Marie Curie-Paris6, Université Denis Diderot-Paris7, F-75252 Paris, France
- ⁵⁸University of Pennsylvania, Philadelphia, Pennsylvania 19104, USA
- ⁵⁹Università di Perugia, Dipartimento di Fisica and INFN, I-06100 Perugia, Italy
- ⁶⁰Università di Pisa, Dipartimento di Fisica, Scuola Normale Superiore and INFN, I-56127 Pisa, Italy
- ⁶¹Prairie View A&M University, Prairie View, Texas 77446, USA
- ⁶²Princeton University, Princeton, New Jersey 08544, USA
- ⁶³Università di Roma La Sapienza, Dipartimento di Fisica and INFN, I-00185 Roma, Italy
- ⁶⁴Universität Rostock, D-18051 Rostock, Germany
- ⁶⁵Rutherford Appleton Laboratory, Chilton, Didcot, Oxon, OX11 0QX, United Kingdom
- ⁶⁶DSM/Dapnia, CEA/Saclay, F-91191 Gif-sur-Yvette, France
- ⁶⁷University of South Carolina, Columbia, South Carolina 29208, USA
- ⁶⁸Stanford Linear Accelerator Center, Stanford, California 94309, USA
- ⁶⁹Stanford University, Stanford, California 94305-4060, USA
- ⁷⁰State University of New York, Albany, New York 12222, USA
- ⁷¹University of Tennessee, Knoxville, Tennessee 37996, USA
- ⁷²University of Texas at Austin, Austin, Texas 78712, USA
- ⁷³University of Texas at Dallas, Richardson, Texas 75083, USA
- ⁷⁴Università di Torino, Dipartimento di Fisica Sperimentale and INFN, I-10125 Torino, Italy
- ⁷⁵Università di Trieste, Dipartimento di Fisica and INFN, I-34127 Trieste, Italy
- ⁷⁶IFIC, Universitat de Valencia-CSIC, E-46071 Valencia, Spain
- ⁷⁷University of Victoria, Victoria, British Columbia, Canada V8W 3P6
- ⁷⁸Department of Physics, University of Warwick, Coventry CV4 7AL, United Kingdom
- ⁷⁹University of Wisconsin, Madison, Wisconsin 53706, USA
- ⁸⁰Yale University, New Haven, Connecticut 06511, USA

(Dated: October 30, 2018)

We study the decays $B^0 \rightarrow J/\psi \pi^+ \pi^-$ and $B^+ \rightarrow J/\psi \pi^+ \pi^0$, including intermediate resonances, using a sample of 382 million $B\bar{B}$ pairs recorded by the BABAR detector at the PEP-II $e^+e^- B$ factory. We measure the branching fractions $\mathcal{B}(B^0 \rightarrow J/\psi \rho^0) = (2.7 \pm 0.3 \pm 0.17) \times 10^{-5}$ and $\mathcal{B}(B^+ \rightarrow J/\psi \rho^+) = (5.0 \pm 0.7 \pm 0.31) \times 10^{-5}$.

We also set the following upper limits at the 90% confidence level: $\mathcal{B}(B^0 \rightarrow J/\psi \pi^+ \pi^- \text{ non-resonant}) < 1.2 \times 10^{-5}$, $\mathcal{B}(B^0 \rightarrow J/\psi f_2) < 4.6 \times 10^{-6}$, and $\mathcal{B}(B^+ \rightarrow J/\psi \pi^+ \pi^0 \text{ non-resonant}) < 4.4 \times 10^{-6}$. We measure the charge asymmetry in charged B decays to $J/\psi \rho$ to be $-0.11 \pm 0.12 \pm 0.08$.

PACS numbers: 13.25.Hw, 12.15.Hh, 11.30.Er

The decay $B^0 \rightarrow J/\psi \rho^0$ [1] can in principle be used to measure the CP violation parameter $\sin 2\beta$. However, the measurement is not as straightforward as for $J/\psi K_S^0$ [2, 3], because it involves the decay of a pseudoscalar meson to two vector mesons, resulting in both CP -odd and CP -even final states. Furthermore, the decay can proceed through either a color-suppressed tree diagram, or a penguin diagram, both shown in Fig. 1, and interference between them could result in direct CP violation [4]. Direct CP violation may also occur in $B^+ \rightarrow J/\psi \rho^+$ decays, where it would manifest itself as a non-zero charge asymmetry:

$$\mathcal{A}_{CP} = \frac{N(B^- \rightarrow J/\psi \rho^-) - N(B^+ \rightarrow J/\psi \rho^+)}{N(B^- \rightarrow J/\psi \rho^-) + N(B^+ \rightarrow J/\psi \rho^+)}. \quad (1)$$

The large intrinsic width of the ρ meson necessitates an analysis of a significant portion of the invariant mass spectrum of the dipion system.

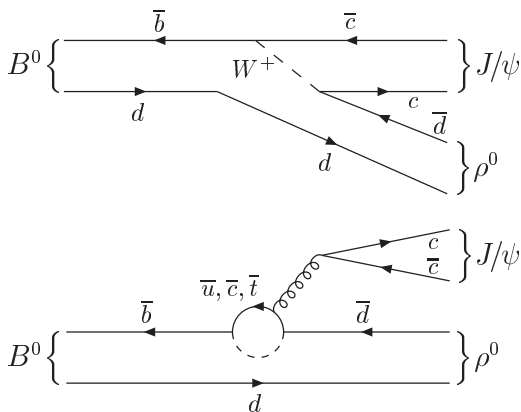


FIG. 1: Tree and penguin diagrams for the process $B^0 \rightarrow J/\psi \rho^0$

The branching fraction for $B^0 \rightarrow J/\psi \pi^+ \pi^-$ has previously been measured at *BABAR* to be $(4.6 \pm 0.7 \pm 0.6) \times 10^{-5}$ [5], including a $J/\psi \rho^0$ component with a branching fraction of $(1.6 \pm 0.6 \pm 0.4) \times 10^{-5}$. This measurement used a data sample containing approximately 56 million $B\bar{B}$ pairs, which is a subset of the sample used in this

analysis. The charged B decay to $J/\psi \rho^+$ has not previously been observed, the *CLEO* collaboration set an upper limit $\mathcal{B}(B^+ \rightarrow J/\psi \rho^+) < 7.7 \times 10^{-4}$ at the 90% confidence level [6].

The data sample used here contains 382 million $B\bar{B}$ pairs collected with the *BABAR* detector at the PEP-II asymmetric-energy e^+e^- storage ring, taken at a center-of-mass (CM) energy equivalent to the mass of the $\Upsilon(4S)$ resonance. An additional data sample, corresponding to an integrated luminosity of 36.8 fb^{-1} , taken at a CM energy 40 MeV below the $\Upsilon(4S)$ resonance, is used to study backgrounds from continuum $q\bar{q}$ production, where $q = u, d, s, c$.

A detailed description of the *BABAR* detector can be found elsewhere [7]. Charged-particle trajectories are measured by a five-layer silicon vertex tracker (SVT) and a 40-layer drift chamber (DCH) operating in a 1.5 T solenoidal magnetic field. A detector of internally reflected Cherenkov light (DIRC) is used for charged hadron identification. Surrounding this is a CsI(Tl) electromagnetic calorimeter (EMC), and finally the instrumented flux return (IFR) of the solenoid, which consists of layers of iron interspersed with resistive plate chambers or limited streamer tubes.

The J/ψ meson is reconstructed in decays to l^+l^- , where l^\pm refers to a charged lepton, e^\pm or μ^\pm . Electrons are selected on the basis of the ratio of EMC shower energy to track momentum, and the energy profile of the EMC shower. For $J/\psi \rightarrow e^+e^-$, an attempt is made to recover energy losses from bremsstrahlung, by looking for showers in the EMC close to those from the electron candidates. This procedure increases the selection efficiency for $J/\psi \rightarrow e^+e^-$ candidates by approximately 30% [8]. The muon selection algorithm uses a neural network, for which the most important input is the number of interaction lengths traversed in the IFR. The lepton pairs are fitted to a common vertex and the invariant mass of the combination is required to be in the range 2.98 (3.06) to 3.14 GeV/c^2 for the e^+e^- ($\mu^+\mu^-$) channels. In order to reduce the background from $B^0 \rightarrow J/\psi K^{*0}$ ($K^{*0} \rightarrow K^+\pi^-$) decays, charged pion candidates are required to satisfy stringent particle identification criteria, based on combined ionization energy loss (dE/dx) in the DCH and SVT with the Cherenkov angle measured in the DIRC.

All tracks are required to originate close to the interaction point, and to lie in polar angle ranges where particle identification efficiency is well measured. The allowed ranges correspond to the geometric acceptances of the DIRC for pions, the EMC for electrons, and the IFR for muons.

Neutral pion candidates are formed by combining pairs

*Deceased

†Also with Università di Perugia, Dipartimento di Fisica, Perugia, Italy

‡Also with Università della Basilicata, Potenza, Italy

§Also with IPPP, Physics Department, Durham University, Durham DH1 3LE, United Kingdom

of isolated showers in the EMC. These are required to spread over a minimum of three crystals, and to have an energy greater than 200 MeV.

To form a B candidate, the reconstructed J/ψ is combined with either a pair of oppositely charged pions, or a charged pion and a π^0 , and a kinematic and geometric fit is used to ensure that all final state particles are consistent with coming from the same decay point. In this fit, we constrain the invariant mass of the l^+l^- and the $\gamma\gamma$ to have the nominal mass of the J/ψ and π^0 , respectively [9]. The energy difference, ΔE , between the candidate energy and the single beam energy, E_{beam}^{CM} , (both in the CM frame) is expected to be close to zero for signal events, and is therefore required to be in the interval -40 to 40 MeV (-60 to 80 MeV) for B^0 (B^+) candidates, corresponding to approximately $\pm 3\sigma$ of the ΔE resolution. Note that the range is asymmetric for B^+ candidates because the π^0 in the final state gives rise to a tail on the low side of the distribution, due to the EMC response to photons. For events where more than one B candidate passes the selection criteria, the candidate with the smallest value of $|\Delta E|$ is chosen.

The branching fraction for each signal channel is obtained from:

$$\mathcal{B} = \frac{N_{sig}}{N_{B\bar{B}} \times \epsilon_{sig} \times \mathcal{B}(J/\psi \rightarrow l^+l^-)}, \quad (2)$$

where N_{sig} and ϵ_{sig} are the observed yield and selection efficiency, respectively, for a specific signal channel, and $N_{B\bar{B}}$ is the number of B meson pairs. We assume that the $\Upsilon(4S)$ decays equally often into neutral and charged B meson pairs. The $J/\psi \rightarrow l^+l^-$ branching fraction is taken to be $(11.87 \pm 0.12)\%$ [9].

We extract the signal yields for the $J/\psi\rho^0$, $J/\psi\pi^+\pi^-$ non-resonant, and $J/\psi f_2$ channels by performing a fit on the sample of reconstructed B^0 candidates. We also perform a similar fit to the sample of charged B candidates in order to obtain the signal yields for the decay channels $B^+ \rightarrow J/\psi\rho^+$ and $B^+ \rightarrow J/\psi\pi^+\pi^0$ non-resonant. The fits are two-dimensional, extended, unbinned maximum likelihood fits to the distributions of m_{ES} and $m_{\pi\pi}$. Seven event categories are considered: (i) $J/\psi\rho$ signal, (ii) $J/\psi\pi\pi$ non-resonant signal, (iii) $J/\psi f_2$ signal, (iv) $J/\psi K_S^0$ events, (v) background events that do not contain a J/ψ (non- J/ψ background), (vi) background events containing a J/ψ (inclusive J/ψ background), and (vii) selected background channels that have been studied in more detail (exclusive J/ψ backgrounds). In the fit to neutral B candidates, the decay channels that comprise category (vii) are $J/\psi K^{*0}$, $J/\psi K^{*+}$, $J/\psi K_1(1270)$, $J/\psi K^+$, $J/\psi\rho^+$ [10], and $J/\psi\pi^+$. For the fit to charged B candidates, the exclusive J/ψ background channels are $J/\psi K^{*0}$, $J/\psi K^{*+}$, $J/\psi K_1(1270)$, $J/\psi K^+$, $J/\psi K_S^0$, and $J/\psi K_L^0$. In both cases, these decay channels are not included in category (vi). Of course, categories (iii) and (iv) are only present in the fit to neutral B candidates.

A probability density function (PDF) is constructed for each category, and the sum of these PDFs is used to

fit the data. The likelihood function for the total sample is the product of the PDF values for each candidate, multiplied by a Poisson factor:

$$\mathcal{L} = \frac{1}{N!} e^{-N'} (N')^N \prod_{i=1}^N \mathcal{P}_i, \quad (3)$$

where N and N' are the numbers of observed and expected events, respectively, and \mathcal{P}_i is the value of the total PDF for event i . For all event categories except for the exclusive J/ψ background, \mathcal{P}_i is a product of one-dimensional PDFs in m_{ES} and $m_{\pi\pi}$.

Fig. 2 shows the m_{ES} and $m_{\pi\pi}$ distributions for the data, and the projections of the PDFs for each category. The functional forms of these PDFs are as follows. For the $J/\psi\rho^0$, $J/\psi\pi^+\pi^-$, $J/\psi f_2$, and $J/\psi K_S^0$ components, the m_{ES} distributions are parametrized by Gaussian functions, all with the same values for the mean and width, which are allowed to float in the fit. In the fit to charged B candidates, a Crystal Ball function [11] is used instead for the m_{ES} distributions of the $J/\psi\rho^+$ and $J/\psi\pi^+\pi^0$ signal components, as the presence of a π^0 in the final state gives rise to a tail on the low mass side of the peak.

The $J/\psi\rho$ signal component is modeled by a relativistic P -wave Breit-Wigner function [12] in $m_{\pi\pi}$:

$$F_\rho(m_{\pi\pi}) = \frac{m_{\pi\pi}\Gamma(m_{\pi\pi})P^{2L_{eff}+1}}{((m_\rho^2 - m_{\pi\pi}^2)^2 + m_\rho^2\Gamma(m_{\pi\pi})^2)}, \quad (4)$$

where $\Gamma(m_{\pi\pi}) = \Gamma_0 \left(\frac{q}{q_0}\right)^3 \left(\frac{m_\rho}{m_{\pi\pi}}\right) \left(\frac{1+R^2q_0^2}{1+R^2q^2}\right)$. The parameter $q(m_{\pi\pi})$ is the pion momentum in the dipion rest frame, with $q_0 = q(m_\rho)$; P is the J/ψ momentum in the B rest frame; L_{eff} is the orbital angular momentum between the J/ψ and the ρ which can be 0, 1 or 2; R is the radius of the Blatt-Weisskopf barrier factor [13, 14], which is taken to be (0.5 ± 0.5) fm, and m_ρ is the ρ meson mass.

The $m_{\pi\pi}$ distribution for the $J/\psi\pi\pi$ non-resonant signal is $F_{\pi\pi} = q(m_{\pi\pi})P^3$, the product of a three-body phase space factor $q(m_{\pi\pi})P$ and a factor P^2 motivated by angular momentum conservation.

For the $J/\psi f_2$ component, the $m_{\pi\pi}$ distribution is described by a relativistic D -wave Breit-Wigner, similar to Eq. 4, but with an extra factor $(q/q_0)^2$ in the expression for $\Gamma(m_{\pi\pi})$.

The decays to $J/\psi K_S^0$ are not considered signal for this analysis. Most of them are removed by the requirement that all tracks are consistent with coming from the same vertex. The $m_{\pi\pi}$ distribution of the remaining $J/\psi K_S^0$ events are modeled by a narrow Gaussian function.

Non- J/ψ background events are modeled by an ARGUS function [15] in m_{ES} . The $m_{\pi\pi}$ PDF is the sum of two Weibull functions [16], and a Breit-Wigner to describe the ρ component of the continuum background. The parameters of this PDF are fixed to values obtained from fits to the J/ψ mass sidebands of the data.

The m_{ES} distribution of the inclusive J/ψ background is an ARGUS function plus a Gaussian at the B mass. The width of this Gaussian is somewhat wider than that used for signal components as it represents B candidates that are not correctly reconstructed. The $m_{\pi\pi}$ PDF is a 4th-order polynomial. The PDF parameters for this component are fixed to values obtained by fits to a large sample of $B \rightarrow J/\psi(\rightarrow l^+l^-)X$ Monte Carlo (MC) simulated events, with signal events and exclusive J/ψ background channels removed.

Each of the exclusive J/ψ background channels is modeled by a two-dimensional PDF derived from the distribution of MC events for that decay channel. The normalizations of these PDFs are determined by taking into account the selection efficiency on MC simulation, and the world average branching fractions [9].

For the branching fraction fit to neutral B candidates there are twelve free parameters: the yields of the $J/\psi\rho$, $J/\psi\pi\pi$, $J/\psi f_2$, $J/\psi K_S^0$, and inclusive J/ψ background components, the mean and width of the Gaussian used for the signal distribution in m_{ES} , the parameters m_ρ , Γ_0 , and L_{eff} in the ρ lineshape, and the mean and width of the $m_{\pi\pi}$ distribution for the $J/\psi K_S^0$ component. All other parameters are fixed, including those describing lineshape of the $f_2(1270)$, the normalizations and shapes of the exclusive J/ψ background PDFs, and the shapes of the inclusive J/ψ and non- J/ψ background PDFs. We also fix the ratio of non- J/ψ to J/ψ (inclusive plus exclusive) background yields to a value obtained from fitting to data in the region $m_{ES} < 5.26$ (i.e. lower in mass than the signal region), and extrapolated to the fit region using distributions from MC simulation.

The configuration for the charged B branching fraction fit is very similar. Here, there are eight free parameters, since there are no $J/\psi K_S^0$ or $J/\psi f_2$ components.

We find from MC simulation studies that correlations between m_{ES} and $m_{\pi\pi}$ give rise to small biases in the numbers of $J/\psi\rho^+$ and $J/\psi\pi^+\pi^0$ non-resonant signal candidates found in the charged B fit. The sizes of these biases are evaluated by examining the distribution of residuals ($N_{obs} - N_{input}$) for a large number of MC experiments, and are listed in Table I. The yields obtained from the branching fraction fit are therefore corrected to take account of this by subtracting these quantities from the fitted yields.

The signal yields and statistical errors obtained from the branching fraction fits are listed in Table I. We also list the statistical significances of the observed signals, $\sqrt{-2\ln(\mathcal{L}_{Null}/\mathcal{L}_{Max})}$, where \mathcal{L}_{Max} is the likelihood from the fit, and \mathcal{L}_{Null} is the value of the likelihood function when the fit is performed with the signal yield constrained to zero events.

We obtain signal efficiencies using samples of MC signal events, produced in monthly blocks so as to match variations in detector and background conditions. Particle identification efficiency is corrected using data control samples of electrons, muons, and pions. The sizes of these corrections vary with momentum and polar an-

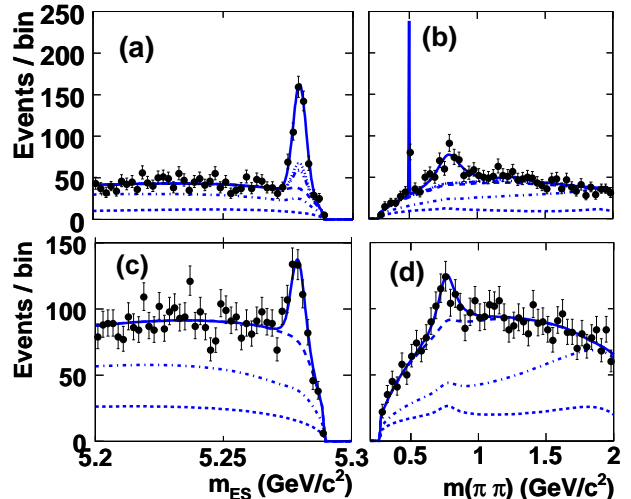


FIG. 2: Distributions of (a) m_{ES} and (b) $m_{\pi\pi}$ for $B^0 \rightarrow J/\psi\pi^+\pi^-$ candidates. The solid line represents the total PDF, while the other lines represent (cumulatively, from the bottom of the plot) non- J/ψ background, inclusive J/ψ background, exclusive J/ψ background, $J/\psi\pi^+\pi^-$ non-resonant signal, and $J/\psi f_2$ signal. The points with error bars represent the data and statistical errors. Plots (c) and (d) show the same distributions for $B^+ \rightarrow J/\psi\pi^+\pi^0$ candidates. The sharp spike in (b) corresponds to $J/\psi K_S^0$ events, while the broader peak is due to $J/\psi\rho^0$ events.

gle, and average corrections are about 1.5% for electrons, 5.9% for muons, and 1.8% for pions. With these corrections applied, about 85% (50%) of electron (muon) pairs, and about 85% of pions, satisfy their respective particle identification requirements. A small, energy-dependent correction (typically about -2% relative) is also applied to decay modes containing a π^0 to account for known differences in photon detection efficiency between data and MC simulation. The corrected signal efficiencies are listed in Table I.

Systematic errors on the branching fraction measurements arise from uncertainties on the signal efficiency, on the fitted yield, on the number of $B^0\bar{B}^0$ or B^+B^- events in the sample, and on the $J/\psi \rightarrow l^+l^-$ branching fraction. The number of $B\bar{B}$ pairs is known to 1.1% accuracy, and an additional 1.6% uncertainty is assigned corresponding to the assumption that the $\Upsilon(4S)$ decays 50% of the time into $B^0\bar{B}^0$ and 50% of the time into B^+B^- [9]. The fractional uncertainty on $\mathcal{B}(J/\psi \rightarrow l^+l^-)$ is 1.0% [9].

The systematic uncertainties on the efficiency are largely due to imperfect simulation of the detector performance. These effects are studied using various data control samples. The largest sources of uncertainty are pion identification efficiency, a 2.0% (3.4%) relative error for charged (neutral) B decay channels, and π^0 efficiency (3% for charged B decays). Tracking efficiency (1.5%) and lepton identification efficiency (1.0%) also contribute

TABLE I: Signal yields, detection efficiencies, and branching fractions for the signal decay channels. The fit bias, product of secondary branching fractions ($\mathcal{B}(J/\psi \rightarrow l^+l^-)$ and $\mathcal{B}(\pi^0 \rightarrow \gamma\gamma)$), and significances of the signals (using statistical uncertainties only) are also listed. The corrected yields are obtained by subtracting the fit bias from the fitted yields. For the yields, efficiencies, and branching fractions, the first errors are statistical and the second are systematic. For decay channels where no significant signal is observed, we quote an upper limit at the 90% confidence level.

Mode	Fit bias (events)	Corrected yield (events)	$\epsilon(\%)$	$\prod \mathcal{B}_i(\%)$	Signif. (σ)	$\mathcal{B}(\times 10^{-5})$
$J/\psi \rho^0$	0	$251.1 \pm 27.5 \pm 11.2$	$20.6 \pm 0.1 \pm 0.8$	11.87 ± 0.12	13.0	$2.7 \pm 0.3 \pm 0.2$
$J/\psi \pi^+ \pi^-$	0	$64.5 \pm 35.5 \pm 7.7$	$20.3 \pm 0.1 \pm 0.8$	11.87 ± 0.12	2.0	< 1.2 (90% C.L.)
$J/\psi f_2$	0	$24.4 \pm 13.8 \pm 1.8$	$20.3 \pm 0.1 \pm 0.8$	11.87 ± 0.12	2.0	< 0.46 (90% C.L.)
$J/\psi \rho^+$	-6.8 ± 1.1	$218.5 \pm 28.8 \pm 9.5$	$9.7 \pm 0.1 \pm 0.4$	11.73 ± 0.12	11.6	$5.0 \pm 0.7 \pm 0.3$
$J/\psi \pi^+ \pi^0$	$+8.2 \pm 0.9$	$-12.7 \pm 27.1 \pm 4.7$	$11.9 \pm 0.1 \pm 0.5$	11.73 ± 0.12	0	< 0.44 (90% C.L.)

to the uncertainty on the efficiency. The polarization of the ρ in $B \rightarrow J/\psi \rho$ decays is unknown. We use an MC sample in which the ρ mesons are unpolarized to obtain the central value of the signal efficiency. We also evaluate the efficiency using MC data samples with different ρ polarizations, and observe a relative variation of 2%, which is assigned as a systematic uncertainty on the branching fraction measurement.

We evaluate the impact of the fit procedure by observing the changes in the yields when varying the PDF parameters that were fixed in the fit within their uncertainties. The resulting differences are added quadratically for sets of parameters that are relatively uncorrelated, and added linearly for highly correlated sets of parameters. We also repeat the fit using alternative functional forms for some PDFs, namely the shape of the inclusive J/ψ background in $m_{\pi\pi}$, and the ρ lineshape, and include the resulting differences in the yield in the systematic uncertainty. In addition, for the $J/\psi \rho^+$ and $J/\psi \pi^+ \pi^0$ channels, systematic uncertainties equal to half of the bias corrections listed in Table I are assigned. The total systematic uncertainties on the yield vary from 1.8 events for the $J/\psi f_2$ channel, to 11.2 events for the $J/\psi \rho^0$ channel.

In order to assess the charge asymmetry \mathcal{A}^ρ , we perform a second fit to the charged B candidate sample. In this fit, all the shape parameters for the signal and background components are fixed to values obtained from the branching fraction fit. This reduces the number of free parameters and improves the reliability of the fit. We include terms for the asymmetries in signal and background components as follows:

$$\begin{aligned}
\mathcal{P}_i &= N^\rho \times \frac{1}{2}(1 - Q_i \mathcal{A}^\rho) \mathcal{P}_i^\rho \\
&+ N^{NR} \times \frac{1}{2}(1 - Q_i \mathcal{A}^{NR}) \mathcal{P}_i^{NR} \\
&+ \sum_j N_j^{bkg} \times \frac{1}{2}(1 - Q_i \mathcal{A}_j^{bkg}) \mathcal{P}_{j,i}^{bkg}, \quad (5)
\end{aligned}$$

where N^ρ , N^{NR} , and N_j^{bkg} are the yields for the $J/\psi \rho^+$ signal, the $J/\psi \pi^+ \pi^0$ non-resonant signal, and the different background components j , respectively, Q_i is the charge of the B candidate in event i , and \mathcal{A}^ρ , \mathcal{A}^{NR} , and \mathcal{A}_j^{bkg} are the corresponding charge asymmetries. The asymmetry parameters for the exclusive J/ψ background

channels are fixed to world average values [9]. The asymmetries for the non- J/ψ background and inclusive J/ψ background components are assumed to be the same ($\mathcal{A}_{inc}^{bkg} = \mathcal{A}_{non}^{bkg} \equiv \mathcal{A}^{bkg}$). This fit therefore has six free parameters: the yields of the $J/\psi \rho^+$ signal, $J/\psi \pi^+ \pi^0$ non-resonant signal, and inclusive J/ψ background components, and the asymmetries \mathcal{A}^ρ , \mathcal{A}^{NR} , and \mathcal{A}^{bkg} .

From the charge asymmetry fit, we obtain $\mathcal{A}^\rho = -0.11 \pm 0.12(\text{stat.})$. The signal and background yields obtained from this fit are entirely consistent with those from the branching fraction fit.

A potential contribution to the systematic uncertainty on the charge asymmetry \mathcal{A}^ρ could come from different pion identification efficiencies for π^+ and π^- , leading to different signal selection efficiencies for positively and negatively charged B candidates. Using data control samples, this effect is found to be negligible.

The other sources of systematic error on the asymmetry are potential differences in the backgrounds for positive and negative B candidates. The parameters describing the charge asymmetries of the exclusive J/ψ background channels are varied within their uncertainties [9], assuming a 10% uncertainty for the $J/\psi K_1(1270)$ channel for which no measurement is available. The normalizations of the exclusive background channels, and the shape parameters of the inclusive J/ψ background and non- J/ψ background components are varied in turn, and the fit is repeated. The resulting changes to the fitted value of \mathcal{A}^ρ are added in quadrature, and the total systematic uncertainty is found to be ± 0.08 .

In summary, we measure the following branching fractions, where the first error in each case is statistical and the second is systematic: $\mathcal{B}(B^0 \rightarrow J/\psi \rho^0) = (2.7 \pm 0.3 \pm 0.2) \times 10^{-5}$, and $\mathcal{B}(B^+ \rightarrow J/\psi \rho^+) = (5.0 \pm 0.7 \pm 0.3) \times 10^{-5}$. The signals for $B^0 \rightarrow J/\psi f_2$, $B^0 \rightarrow J/\psi \pi^+ \pi^-$ non-resonant, and $B^+ \rightarrow J/\psi \pi^+ \pi^0$ non-resonant are not statistically significant, thus we set the following upper limits at the 90% confidence level: $\mathcal{B}(B^0 \rightarrow J/\psi f_2) < 4.6 \times 10^{-6}$, $\mathcal{B}(B^0 \rightarrow J/\psi \pi^+ \pi^-) < 1.2 \times 10^{-5}$, and $\mathcal{B}(B^+ \rightarrow J/\psi \pi^+ \pi^0) < 4.4 \times 10^{-6}$. These values are calculated by summing the statistical and systematic uncertainties in quadrature, multiplying the result by 1.28, and adding it to the central value of the branching fraction. We measure the charge asymmetry defined in Eq. 1 for the decays $B^\pm \rightarrow J/\psi \rho^\pm$, $\mathcal{A}^\rho = -0.11 \pm 0.12 \pm 0.08$.

We are grateful for the excellent luminosity and machine conditions provided by our PEP-II colleagues, and for the substantial dedicated effort from the computing organizations that support *BABAR*. The collaborating institutions wish to thank SLAC for its support and kind hospitality. This work is supported by DOE and NSF (USA), NSERC (Canada), IHEP (China), CEA and

CNRS-IN2P3 (France), BMBF and DFG (Germany), INFN (Italy), FOM (The Netherlands), NFR (Norway), MIST (Russia), MEC (Spain), and PPARC (United Kingdom). Individuals have received support from the Marie Curie EIF (European Union) and the A. P. Sloan Foundation.

-
- [1] Charge conjugation is implied throughout this letter unless stated otherwise.
- [2] *BABAR* Collaboration, B. Aubert *et al.*, Phys. Rev. Lett. **94**, 161803 (2005).
- [3] Belle Collaboration, K. Abe *et al.*, Phys. Rev. D **71**, 072003 (2005) [Erratum-ibid. D **71**, 079903 (2005)]
- [4] I. Dunietz, Phys. Lett. B **316**, 561 (1993).
- [5] *BABAR* Collaboration, B. Aubert *et al.*, Phys. Rev. Lett. **90**, 091801 (2003).
- [6] CLEO Collaboration, M. Bishai *et al.*, Phys. Lett. B **369**, 186 (1996).
- [7] *BABAR* Collaboration, B. Aubert *et al.*, Nucl. Instrum. Methods Phys. Res., Sect. A **479**, 1 (2002).
- [8] B. Aubert *et al.* [*BABAR* Collaboration], Phys. Rev. D **65**, 032001 (2002)
- [9] W.-M. Yao *et al.*, J. Phys. G **33**, 1 (2006).
- [10] Note that the $J/\psi \rho^+$ channel which is being measured in this note is one of the exclusive J/ψ background channels in the fit to neutral B candidates. For the purpose of choosing the normalization for this PDF, we assume a value of $(6.0 \pm 6.0) \times 10^{-5}$ for the branching fraction.
- [11] M.J.Oreglia, Ph.D Thesis, SLAC-236(1980), Appendix D; J.E.Gaiser, Ph.D Thesis, SLAC-255(1982), Appendix F; T.Skwarnicki, Ph.D Thesis, DESY F31-86-02(1986), Appendix E.

The Crystal Ball function can be written as:

$$CB(m) = \begin{cases} \exp\left(-\frac{(m-\mu)^2}{2\sigma^2}\right) & m > \mu - \alpha\sigma \\ \frac{(n/\alpha)^n \exp(-\alpha^2/2)}{((\mu-m)/\sigma + n/\alpha - \alpha)^n} & m < \mu - \alpha\sigma \end{cases}$$

- where μ is the mean value, σ is a measure of the width, and n and α are parameters describing the tail.
- [12] J. Pisut and M. Roos, N. Phys. B **6**, 325 (1968).
- [13] J. M. Blatt and V. F. Weisskopf, *Theoretical Nuclear Physics* (Wiley, New York, 1952), p. 361.
- [14] Values for the barrier radius can be estimated from $q\bar{q}$ meson models (S. Godfrey and N. Isgur, Phys. Rev. D **32**, 189 (1985) : figure 12), and by fits to experimental data (see for example D. Aston *et al.*, Nucl. Phys. B **296**, 493 (1988)).
- [15] ARGUS Collaboration, H. Albrecht *et al.*, Z. Phys. C **48**, 543 (1990).

The ARGUS function can be written as

$$A(m) = y\sqrt{1-y^2} \exp(\xi(1-y^2)) \quad y < 1 \\ A(m) = 0 \quad y > 1$$

where ξ is a shape parameter, $y = m/m_{max}$ and m_{max} is a kinematic limit, equal in this case to half the total CM energy.

- [16] The Weibull function can be written as

$$W(m) = CV(m - M_{on})^{(C-1)} \exp[-V(m - M_{max})^C],$$

where $V = (C-1)/(C(M_{max} - M_{on})^C)$. M_{max} is the position of the function maximum, M_{on} is the lower kinematic cut-off, and C is a shape parameter.